

Learning the CSI Denoising and Feedback Without Supervision

Valentina Rizzello and Wolfgang Utschick
Department of Electrical and Computer Engineering
Technical University of Munich
{valentina.rizzello, utschick}@tum.de

Abstract—In this work, we develop a joint denoising and feedback strategy for channel state information in frequency division duplex systems. In such systems, the biggest challenge is the overhead incurred when the mobile terminal has to send the downlink channel state information or corresponding partial information to the base station, where the complete estimates can subsequently be restored. To this end, we propose a novel learning-based framework for denoising and compression of channel estimates. Unlike existing studies, we extend a recently proposed approach and show that based solely on noisy uplink data available at the base station, it is possible to learn an autoencoder neural network that generalizes to downlink data. Subsequently, half of the autoencoder can be offloaded to the mobile terminals to generate channel feedback there as efficiently as possible, without any training effort at the terminals or corresponding transfer of training data. Numerical simulations demonstrate the excellent performance of the proposed method.

Index Terms—Machine learning, Massive MIMO, FDD systems, Autoencoders, Denoising, Deep learning.

I. INTRODUCTION

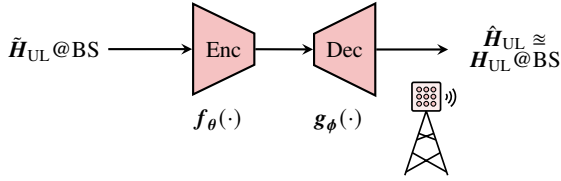
Massive multiple-input multiple-output (MIMO) is certainly the most noticeable technology to increase the throughput and guarantee reliability in modern and future wireless communication systems [1]. With the deployment of large-scale antenna arrays, space diversity induces a remarkable improvement in the spectral efficiency and makes possible to serve multiple users at the same time. However, to benefit from all the prospective advantages of massive MIMO, the high dimensional channel frequency response must be accurate and promptly acquired at the base station (BS). Therefore, the strong reciprocity between the corresponding uplink (UL) and downlink (DL) channels makes time division duplex (TDD) networks one of the most prominent solution candidates under these strict constraints [2]. In contrast, in frequency division duplex (FDD) systems, the absence of reciprocity between the UL and DL channel responses and consequently the huge overhead for reporting the channel state information (CSI) from the mobile terminal (MT) to the BS represents the major limitation for an effective deployment of massive MIMO communications. Although the TDD operation mode is the most commonly adopted, it has been shown that FDD massive MIMO would handle the low latency requirements

imposed by the standardization potentially much better than TDD solutions [3]. Hence, this premise has motivated and encouraged several studies that aim to reduce or eliminate the DL CSI acquisition overhead. In addition to some well-known examples based on a particular model and sparsity assumptions that show how to extrapolate DL covariance from UL covariance [4], there are a variety of data-driven approaches that address the challenge of recovering instantaneous DL CSI in FDD systems at the BS. Among these, to eliminate the need for feedback, several machine learning approaches have been proposed based on supervised learning of direct extrapolation of CSI across the frequency gap, based on pairs of UL–DL training data [5]–[10].

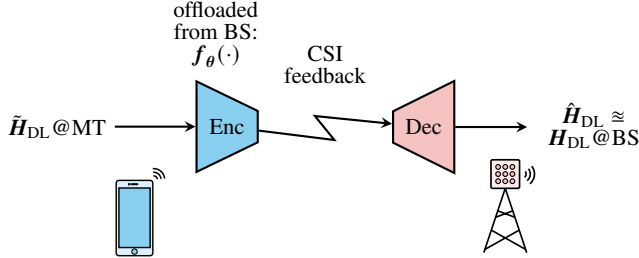
A very innovative solution is represented by the concept of autoencoder neural networks which are trained in order to learn a low rate feedback from the MT to the BS [11]–[16]. In this setup, the DL CSI is encoded at the MT into a codeword, which is then fed back to the BS and decoded there, implying a distributed implementation of the parts of the autoencoder at the MT and BS.

In this work, following this general approach, we propose a novel method which is again based on the autoencoding concept. However, motivated by the results in [17], the unsupervised training of the autoencoder is conducted at the BS solely based on noisy UL training data, thus avoiding the issue that collecting DL data at the BS to enable the training otherwise would require an immense effort with respect to the overall network traffic. By the corresponding result from [17], we mean the equivalence of UL and DL CSI discovered therein with respect to their probability distributions. Thus, the core idea of our scheme is that the neural network encoder trained on UL data at the BS can be applied to DL data without any further adaptation, from any mobile device to which the encoder is offloaded. Training on the MT is no longer necessary at all, making it possible to quickly update the encoder on the MT at any time and place, e.g., when moving from one cell to another or for different locations in the cell. Compared to our approach, training at the MT with DL data has some disadvantages, e.g.: *i*) the MT could spend only a short amount of time inside a cell and could not collect enough samples for training, *ii*) if multiple MTs stayed in the same cell long enough to perform the training of different autoencoders, lots of computational power would be wasted since only one decoder would be deployed at the

This research was supported by an unrestricted gift from Futurewei Technologies, Inc., Huawei R&D USA.



(a) Training of the autoencoder at the BS.



(b) Codeword generation at the MT.

Fig. 1. Training of the autoencoder based on UL CSI at the BS, generation of the codeword by the offloaded encoder at the MT, transmission over the radio channel, and subsequent reconstruction of the DL CSI at the BS.

BS, *iii*) there would be a high risk of overfitting since it's unlikely that a MT visits all the locations in a cell because of the systematic behaviour of the users. Based on the presented simulation results, we are eventually able to demonstrate the excellent performance of the proposed technique.

II. SYSTEM ARCHITECTURE

In the following, we indicate with $\tilde{\mathbf{H}}_{\text{UL}}$ and $\tilde{\mathbf{H}}_{\text{DL}} \in \mathbb{C}^{N_a \times N_c}$ the noisy UL and DL CSI matrices of the transmission channel between the BS and the single antenna MT, where N_a and N_c denote the number of antennas at the BS and the number of subcarriers, respectively. In addition, we can express $\tilde{\mathbf{H}}_{\text{UL}}$ as

$$\tilde{\mathbf{H}}_{\text{UL}} = \mathbf{H}_{\text{UL}} + \mathbf{N}, \quad (1)$$

where \mathbf{H}_{UL} and $\mathbf{N} \in \mathbb{C}^{N_a \times N_c}$ represents the true UL CSI matrix and the additive white Gaussian noise, respectively. Analogous expressions can be derived for $\tilde{\mathbf{H}}_{\text{DL}}$. Note that throughout this work we assume that the true data for both UL and DL, namely \mathbf{H}_{UL} and \mathbf{H}_{DL} , are inaccessible and only a noisy version of them is available. The proposed method consists of two phases, which are illustrated in Fig. 1. First, an autoencoder $\mathbf{g}_\phi(\mathbf{f}_\theta(\cdot))$ is trained at the BS based solely on noisy UL data $\tilde{\mathbf{H}}_{\text{UL}}$, which is supposed to be collected during the standard UL operation of the BS in advance. The \mathbf{f}_θ denotes the encoder with parameters θ and \mathbf{g}_ϕ denotes the decoder with parameters ϕ , see Fig. 1a. It is well-known that autoencoders implicitly introduce regularization for the reconstruction of the input signal, cf. [18] for an introduction to the fundamentals behind denoising with deep neural networks. In essence, an autoencoder can be trained with the noisy data $\tilde{\mathbf{H}}_{\text{UL}}$ in an unsupervised fashion to obtain an estimate $\hat{\mathbf{H}}_{\text{UL}}$ which will be approximately equal to the unknown \mathbf{H}_{UL} . It should be noted that for the proposed method, there are no special requirements for the acquisition of the UL training data, except for the property that they come from the same propagation scenario as

the subsequent DL data to which the encoder will be applied at the MTs. Subsequently, half of the autoencoder, namely the encoding part $\mathbf{f}_\theta(\cdot)$, is offloaded to the MT based on a respective network protocol, which is due to space restriction not further considered here.

In the second phase, similarly to what has been proposed in [17], we reuse the UL-trained autoencoder neural network for the recovery of the complete DL CSI. In particular, each MT takes the noisy DL CSI estimate $\tilde{\mathbf{H}}_{\text{DL}}$ and feeds it into the offloaded UL-trained encoder to obtain the latent vector or codeword \mathbf{z}_{DL} . Then, the codeword is fed back to the BS which recovers $\hat{\mathbf{H}}_{\text{DL}} \approx \mathbf{H}_{\text{DL}}$ with the second half of the autoencoder, namely the UL-trained decoder.

III. DATASET DESCRIPTION

Our study is based on a single urban microcell (UMi) with 150 meters radius, which has been simulated with the MATLAB based software QuaDRiGa version 2.2 [19], [20]. Specifically, we consider non-line-of-sight (NLoS) channels, with $L = 58$ multi-path components (MPCs), which means a rich scattering propagation environment. The BS is placed at a height of 10 meters and is equipped with a uniform planar array (UPA) with $N_a = 8 \times 8$ “3GPP-3d” antennas, while the users have a single omni-directional antenna each. In addition, the BS antennas are tilted by 6 degrees towards the ground to point in the direction of the users. The UL center frequency is 2.5 GHz while the DL center frequencies are 2.62 GHz, and 2.98 GHz, which correspond to a FDD gap of 120 MHz and 480 MHz, respectively. For each frequency, we consider a bandwidth of approximately 8 MHz divided over $N_c = 160$ subcarriers. The cell has been sampled at 60×10^3 different locations of MT and for each sample the channels at the predefined frequencies are collected. Therefore, the dataset is split into three groups of 48×10^3 , 6×10^3 and 6×10^3 samples, where each sample consists of the three matrices \mathbf{H}_{UL} , $\mathbf{H}_{\text{DL-120}}$, and $\mathbf{H}_{\text{DL-480}} \in \mathbb{C}^{N_a \times N_c}$. Note again that although the training of the autoencoder at the BS is based solely on the UL CSI, it still covers the distribution of the unseen DL CSI as well, since the UL and DL data ultimately follow the same propagation scenario, cf. [17]. With respect to testing, only the test set of the two DL CSI datasets (DL@120, 480) will be used. Additionally, and likewise [17] the channels are normalized with respect to their path-gain.

IV. AUTOENCODER

An autoencoder is a neural network that is trained in an unsupervised fashion to reconstruct its input. It has been introduced in [21] and its purpose is to find a compact representation of the data. The autoencoder consists of two parts: an encoder function \mathbf{f}_θ with hyperparameters θ and a decoder function \mathbf{g}_ϕ with hyperparameters ϕ . The encoder projects a d -dimensional input vector \mathbf{x} into a typically lower dimensional latent space representation $\mathbf{z} \in \mathbb{C}^{d_z}$ with $d_z \ll d$, whereas the decoder reconstructs the original input from \mathbf{z} , i.e.,

$$\mathbf{x} \xrightarrow{\mathbf{f}_\theta} \mathbf{z} \xrightarrow{\mathbf{g}_\phi} \hat{\mathbf{x}} \approx \mathbf{x}. \quad (2)$$

TABLE I
ENCODER ARCHITECTURE.

| Layer type | Output shape | #Parameters θ |
|---------------------|--------------------------|----------------------|
| Input | $64 \times 160 \times 2$ | 0 |
| Conv2D, strides=2 | $32 \times 80 \times 8$ | 152 |
| Batch normalization | $32 \times 80 \times 8$ | 32 |
| ReLU | $32 \times 80 \times 8$ | 0 |
| Conv2D, strides=2 | $16 \times 40 \times 16$ | 1168 |
| Batch normalization | $16 \times 40 \times 16$ | 64 |
| ReLU | $16 \times 40 \times 16$ | 0 |
| Conv2D, strides=2 | $8 \times 20 \times 32$ | 4640 |
| Batch normalization | $8 \times 20 \times 32$ | 128 |
| ReLU | $8 \times 20 \times 32$ | 0 |
| Conv2D, strides=2 | $4 \times 10 \times 64$ | 18496 |
| Batch normalization | $4 \times 10 \times 64$ | 256 |
| ReLU | $4 \times 10 \times 64$ | 0 |
| Conv2D, strides=2 | $2 \times 5 \times 128$ | 73856 |
| Batch normalization | $2 \times 5 \times 128$ | 512 |
| ReLU | $2 \times 5 \times 128$ | 0 |
| Flatten | 1280 | 0 |
| Fully-connected | 256 | 327936 |
| Tanh | 256 | 0 |

TABLE II
DECODER ARCHITECTURE.

| Layer type | Output shape | #Parameters ϕ |
|------------------------------|--------------------------|--------------------|
| Input | 256 | 0 |
| Fully-connected | 1280 | 328960 |
| Reshape | $2 \times 5 \times 128$ | 0 |
| Conv2D transposed, strides=2 | $4 \times 10 \times 128$ | 147584 |
| Batch normalization | $4 \times 10 \times 128$ | 512 |
| ReLU | $4 \times 10 \times 128$ | 0 |
| Conv2D transposed, strides=2 | $8 \times 20 \times 64$ | 73792 |
| Batch normalization | $8 \times 20 \times 64$ | 256 |
| ReLU | $8 \times 20 \times 64$ | 0 |
| Conv2D transposed, strides=2 | $16 \times 40 \times 32$ | 18464 |
| Batch normalization | $16 \times 40 \times 32$ | 128 |
| ReLU | $16 \times 40 \times 32$ | 0 |
| Conv2D transposed, strides=2 | $32 \times 80 \times 16$ | 4624 |
| Batch normalization | $32 \times 80 \times 16$ | 64 |
| ReLU | $32 \times 80 \times 16$ | 0 |
| Conv2D transposed, strides=2 | $64 \times 160 \times 8$ | 1160 |
| Batch normalization | $64 \times 160 \times 8$ | 32 |
| ReLU | $64 \times 160 \times 8$ | 0 |
| Conv2D transposed | $64 \times 160 \times 2$ | 146 |

Note that the bottleneck or hourglass structure of the architecture is a key element of the autoencoding concept, as it forces the network to learn only the important features that allow reconstruction with the decoder, cf. [22] and [23].

For the proposed autoencoder in this work, we use a deep neural network with several convolutional layers. The encoder and decoder architectures are described in Tables I and II. Firstly, the real and imaginary parts of the original noisy UL matrix $\tilde{\mathbf{H}}_{\text{UL}} \in \mathbb{C}^{64 \times 160}$ have been stacked along the third dimension to form a real-valued tensor $\tilde{\mathbf{H}}_{\text{UL}}^{\text{real}} \in \mathbb{R}^{64 \times 160 \times 2}$, which represents the input of the encoder. By observing the encoder in Table I, we can distinguish five consecutive blocks, each of them formed by the cascade of a convolutional layer, a batch normalization layer [24], and the rectified linear unit (ReLU) activation function. A key attribute of this architecture is to use strided convolutions [25] which are meant to progressively extract features and reduce the input dimension

down to 1280 units. After the progressive reduction of the input dimension, a fully connected layer with $\tanh(\cdot)$ activation functions completes the encoder and generates the codeword \mathbf{z}_{UL} , which is a real valued vector with $d_z = 256$ dimensions that leads to a compression factor of

$$\frac{64 \times 160 \times 2}{256} = 80. \quad (3)$$

Note that having a deep architecture with multiples strided convolutional layers before the fully connected layer helps to substantially reduce the total number of trainable parameters which is highly affected by the number of parameters in the fully connected layer. The decoder, which is displayed in Table II, is supposed to map the codeword back to the original input $\tilde{\mathbf{H}}_{\text{UL}}^{\text{real}}$, thereby benefiting from the regularizing effect (denoising) of the autoencoder concept. Its structure is equal to the mirrored version of the encoder, where deconvolutions are in place of convolutions and a final transposed convolution with two feature maps recovers the original input shape. Despite the large size, this autoencoder architecture has a number of trainable parameters which is smaller compared to autoencoders built with the same principle of CsiNet [11].

V. SIMULATIONS

The autoencoder neural network has been implemented with Tensorflow [26] and single-precision has been utilized for the training. We consider mini-batches of 64 samples and we use the Adam optimization algorithm [27] to tune the hyperparameters θ and ϕ of the neural network. The weights are updated in order to minimize an empirical risk function based on the least-squares loss function

$$\mathcal{L}(\theta, \phi) = \left\| \mathbf{g}_{\phi} \left(\mathbf{f}_{\theta} \left(\tilde{\mathbf{H}}_{\text{UL}}^{\text{real}} \right) \right) - \tilde{\mathbf{H}}_{\text{UL}}^{\text{real}} \right\|^2. \quad (4)$$

The UL-trained encoder is then used at each MT to generate the codeword \mathbf{z}_{DL} from the noisy DL CSI estimate $\tilde{\mathbf{H}}_{\text{DL}}$. The codeword is then sent to the BS, which uses the UL-trained decoder to obtain a clean version of the DL CSI $\hat{\mathbf{H}}_{\text{DL}} \approx \mathbf{H}_{\text{DL}}$.

After the training, we measure the quality of the unsupervised denoising in terms of normalized mean square error ε^2 and cosine similarity ρ , where

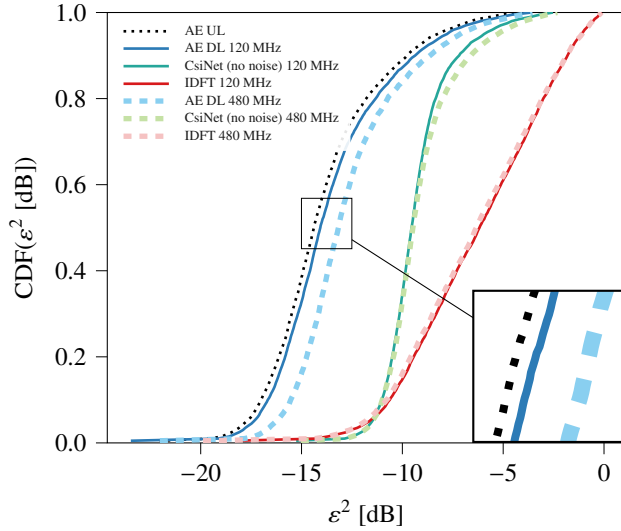
$$\varepsilon^2 = \mathbb{E} \left[\frac{\|\hat{\mathbf{H}} - \mathbf{H}\|_{\text{F}}^2}{\|\mathbf{H}\|_{\text{F}}^2} \right] \quad (5)$$

and

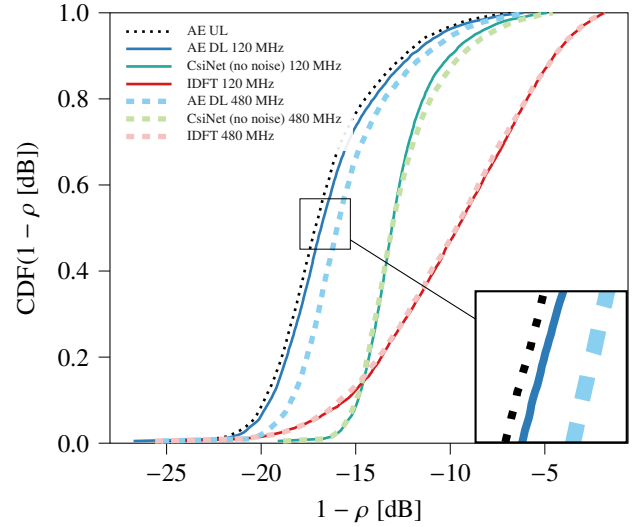
$$\rho = \mathbb{E} \left[\frac{1}{N_c} \sum_{n=1}^{N_c} \frac{|\hat{\mathbf{h}}_n^{\text{H}} \mathbf{h}_n|}{\|\hat{\mathbf{h}}_n\|_2 \|\mathbf{h}_n\|_2} \right], \quad (6)$$

being $\mathbf{H} \in \mathbb{C}^{N_a \times N_c}$ the true CSI, and \mathbf{h}_n its n -th column, and $\hat{\mathbf{H}}$ and $\hat{\mathbf{h}}_n$ their corresponding versions at the decoder output.

In addition, we also evaluate the performance in terms of average per-user rate with zero forcing precoding. To this end, we consider two different values of SNR, namely 10 dB and 0 dB, where the SNR represents the level of CSI corruption, i.e., $\mathbb{E}[\|\mathbf{H}\|_{\text{F}}^2 / \|N\|_{\text{F}}^2]$. We further compare the results achieved with the UL-trained autoencoder with two methods that serve as a reference. In particular, we utilize the CsiNet method,



(a) CDFs NMSE.



(b) CDFs Cosine Similarity.

Fig. 2. CDFs performance metrics of different methods for SNR = 10 dB.

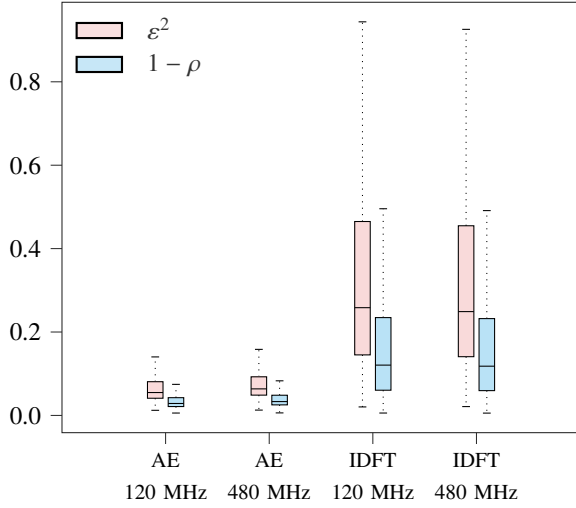


Fig. 3. Performance metrics of AE vs. IDFT for SNR = 0 dB.

which requires a learning-phase and has been proposed in [11], and another method which is based on the IDFT which does not require any learning. CsiNet is based on an autoencoder approach trained on DL CSI that exploits the sparsity of CSI in the space-delay domain, and is often used as a benchmark. After transforming the DL CSI in the space-delay domain, the authors in [11] propose to retain only a small fraction of the component in the time domain, being the remaining component close to zero, and to train an autoencoder with this “cropped” version of the CSI. Specifically, we keep 64 out of 160 time-delay instances, and to be consistent with the original paper, only for the CsiNet results, we decide not to add any noise to the DL CSI.

For the approach based on the IDFT, first we transform the noisy DL CSI $\hat{\mathbf{H}}_{\text{DL}}$ to the space-delay domain by a multiplication with a DFT matrix. Then, we only keep the

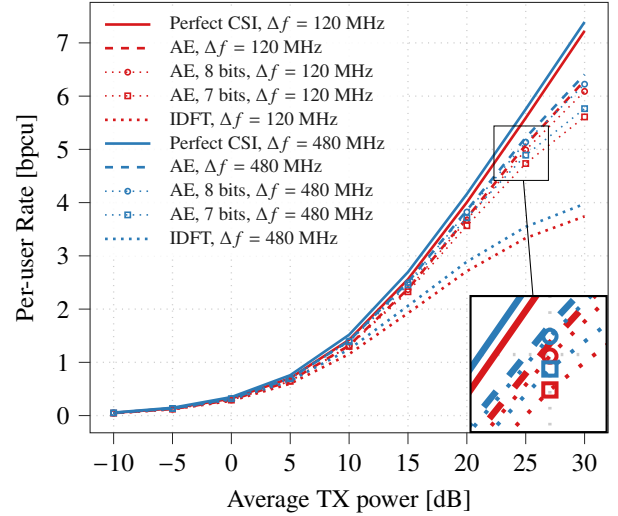


Fig. 4. Per-user rate performance with LISA of DL CSI for $\mathbb{E}[\|\mathbf{H}\|_{\text{F}}^2/\|N\|_{\text{F}}^2] = 10$ dB and a multi-user scenario with 8 users.

first two columns in the space-time domain, such that the total number of coefficients is 256, as it is assumed for the codeword. Afterwards, these coefficients are sent to the BS, which reconstructs the DL CSI in the space-frequency domain, by operating the zero-padding followed by the DFT transformation. The results of NMSE and cosine similarity for SNR = 10 dB are displayed in the subplots of Fig. 2. We can clearly observe that the UL-trained autoencoder (“AE DL 120 MHz”, “AE DL 480 MHz”) performs very well on DL data too, with only a slight drop in performance when increasing the frequency gap from 120 MHz to 480 MHz. The “AE UL” curve demonstrates the reconstruction property of the autoencoder when applied to UL data, which serves as a further reference. Note that the other “AE”-labeled solutions have never seen training samples of DL CSI. Nevertheless, it

can be observed that the “AE” solutions show considerable gain compared to the “IDFT” method and still some gain compared to the “CsiNet” curve. Analogous conclusions can be made by observing the performance metrics in Fig. 3 for SNR = 0 dB where the NMSE and cosine similarity achieved with our approach are compared with those of the IDFT approach.

Finally, results of the average per-user rate in a multi-user scenario with 8 users are discussed. Likewise [17], we adopt the LISA algorithm [28] which is applied independently on each of the 160 carriers, and the results are then averaged over the carriers. Fig. 4 shows the per-user rate for 120 and 480 MHz frequency gaps, averaged over 100 instances of LISA simulation runs for $\mathbb{E}[\|\mathbf{H}\|_{\text{F}}^2/\|\mathbf{N}\|_{\text{F}}^2] = 10$ dB. The continuous lines represent the rates achievable with perfect DL CSI knowledge, the dashed lines represent the rates obtained with the DL CSI predicted with the same UL-trained autoencoder at each MT, and the dotted lines represent the rates with the IDFT method. We can observe that the rates per-user with the DL channels denoised with the AE is extremely close to the rates achieved with the true DL CSI and that there is a significant gain compared to the IDFT method. Furthermore, we only notice a moderate degradation in the per-user rate when we apply uniform 8 bit (7-bit) quantization to each element of the codewords, so that the total number of bits to be sent over the return channel is $256 \times 8 = 2048$ bits ($256 \times 7 = 1792$ bits). Note that the quantization of the codewords can be easily performed because the activation function at the end of the encoder forces the codeword values into the interval $[-1, 1]$.

VI. CONCLUSIONS

In this work, following the idea of using autoencoders for noise reduction and codeword generation for DL CSI in FDD systems, we presented a novel concept. This is based on the recently discovered equivalence of UL and DL data across the FDD frequency gap, which allows training the autoencoder at the BS instead of the MT, followed by offloading the same encoder to each MT. Training on the MT is no longer necessary, making it possible to quickly update the encoder on the MT at any time and place. The promising results presented validate our proposed method.

REFERENCES

- [1] T. L. Marzetta, “Noncooperative Cellular Wireless with Unlimited Numbers of Base Station Antennas,” *IEEE Trans. Wireless Commun.*, vol. 9, no. 11, pp. 3590–3600, 2010.
- [2] L. Sanguinetti, E. Björnson, and J. Hoydis, “Toward Massive MIMO 2.0: Understanding Spatial Correlation, Interference Suppression, and Pilot Contamination,” *IEEE Trans. Commun.*, vol. 68, no. 1, pp. 232–257, 2020.
- [3] E. Björnson, E. G. Larsson, and T. L. Marzetta, “Massive MIMO: ten myths and one critical question,” *IEEE Commun. Mag.*, vol. 54, no. 2, pp. 114–123, 2016.
- [4] M. Barzegar Khalilsarai, S. Haghghatshoar, X. Yi, and G. Caire, “FDD massive MIMO via UL/DL channel covariance extrapolation and active channel sparsification,” *IEEE Trans. Wireless Commun.*, vol. 18, no. 1, pp. 121–135, 2019.
- [5] M. Arnold, S. Dörner, S. Cammerer, S. Yan, J. Hoydis, and S. ten Brink, “Enabling FDD massive MIMO through deep learning-based channel prediction,” *CoRR*, vol. abs/1901.03664, 2019.

- [6] M. Alrabeiah and A. Alkhateeb, “Deep Learning for TDD and FDD Massive MIMO: Mapping Channels in Space and Frequency,” in *2019 53rd Asilomar Conference on Signals, Systems, and Computers*, 2019, pp. 1465–1470.
- [7] J. Wang, Y. Ding, S. Bian, Y. Peng, M. Liu, and G. Gui, “UL-CSI data driven deep learning for predicting DL-CSI in cellular fdd systems,” *IEEE Access*, vol. 7, pp. 96 105–96 112, 2019.
- [8] Y. Han, M. Li, S. Jin, C. K. Wen, and X. Ma, “Deep Learning-Based FDD Non-Stationary Massive MIMO Downlink Channel Reconstruction,” *IEEE J. Sel. Areas Commun.*, vol. 38, no. 9, pp. 1980–1993, 2020.
- [9] M. S. Safari, V. Pourahmadi, and S. Sodagari, “Deep UL2DL: Data-Driven Channel Knowledge Transfer From Uplink to Downlink,” *IEEE Open Journal of Vehicular Technology*, vol. 1, pp. 29–44, 2020.
- [10] V. Rizzello, I. Brayek, M. Joham, and W. Utschick, “Learning the Channel State Information Across the Frequency Division Gap in Wireless Communications,” in *WSA 2020; 24th International ITG Workshop on Smart Antennas*, 2020, pp. 1–6.
- [11] C. Wen, W. Shih, and S. Jin, “Deep learning for massive MIMO CSI feedback,” *IEEE Wireless Commun. Lett.*, vol. 7, no. 5, pp. 748–751, 2018.
- [12] Z. Liu, L. Zhang, and Z. Ding, “Exploiting bi-directional channel reciprocity in deep learning for low rate massive MIMO CSI feedback,” *IEEE Wireless Commun. Lett.*, vol. 8, no. 3, pp. 889–892, 2019.
- [13] —, “An efficient deep learning framework for low rate massive MIMO CSI reporting,” *IEEE Trans. Commun.*, vol. 68, no. 8, pp. 4761–4772, 2020.
- [14] J. Guo, C. Wen, S. Jin, and G. Y. Li, “Convolutional neural network-based multiple-rate compressive sensing for massive MIMO CSI feedback: Design, simulation, and analysis,” *IEEE Trans. Wireless Commun.*, vol. 19, no. 4, pp. 2827–2840, 2020.
- [15] J. Guo, C. K. Wen, and S. Jin, “Deep learning-based CSI feedback for beamforming in single- and multi-cell massive MIMO systems,” *IEEE J. Sel. Areas Commun.*, pp. 1–1, 2020.
- [16] F. Sohrabi, K. M. Attiah, and W. Yu, “Deep learning for distributed channel feedback and multiuser precoding in FDD massive MIMO,” *IEEE Trans. Wireless Commun.*, pp. 1–1, 2021.
- [17] W. Utschick, V. Rizzello, M. Joham, Z. Ma, and L. Piazzini, “Learning the CSI Recovery in FDD Systems,” 2021.
- [18] R. Heckel, W. Huang, P. Hand, and V. Voroninski, “Rate-optimal denoising with deep neural networks,” *Information and Inference: A Journal of the IMA*, 06 2020, iaaa011.
- [19] S. Jaeckel, L. Raschkowski, F. Burkhardt, and L. Thiele, “Efficient Sum-of-Sinusoids-Based Spatial Consistency for the 3GPP New-Radio Channel Model,” in *2018 IEEE Globecom Workshops (GC Wkshps)*, 2018, pp. 1–7.
- [20] M. Kurras, S. Dai, S. Jaeckel, and L. Thiele, “Evaluation of the Spatial Consistency Feature in the 3GPP Geometry-Based Stochastic Channel Model,” in *2019 IEEE Wireless Communications and Networking Conference (WCNC)*, 2019, pp. 1–6.
- [21] D. E. Rumelhart, G. E. Hinton, and R. J. Williams, *Learning Internal Representations by Error Propagation*. Cambridge, MA, USA: MIT Press, 1986, p. 318–362.
- [22] I. Goodfellow, Y. Bengio, and A. Courville, *Deep Learning*. MIT Press, 2016, <http://www.deeplearningbook.org>.
- [23] D. Bank, N. Koenigstein, and R. Giryes, “Autoencoders,” 2021.
- [24] S. Santurkar, D. Tsipras, A. Ilyas, and A. Madry, “How does batch normalization help optimization?” in *Advances in Neural Information Processing Systems 31: Annual Conference on Neural Information Processing Systems 2018, NeurIPS 2018, December 3-8, 2018, Montréal, Canada*, S. Bengio and et al, Eds., 2018, pp. 2488–2498.
- [25] J. T. Springenberg, A. Dosovitskiy, T. Brox, and M. A. Riedmiller, “Striving for simplicity: The all convolutional net,” in *3rd International Conference on Learning Representations, ICLR 2015, San Diego, CA, USA, May 7-9, 2015, Workshop Track Proceedings*, Y. Bengio and Y. LeCun, Eds., 2015.
- [26] M. Abadi et al, “TensorFlow: Large-Scale Machine Learning on Heterogeneous Systems,” 2015, software available from tensorflow.org.
- [27] D. P. Kingma and J. Ba, “Adam: A Method for Stochastic Optimization,” in *3rd International Conference on Learning Representations, ICLR 2015, San Diego, CA, USA, May 7-9, 2015, Conference Track Proceedings*, Y. Bengio and Y. LeCun, Eds., 2015.
- [28] W. Utschick, C. Stöckle, M. Joham, and J. Luo, “Hybrid LISA Precoding for Multiuser Millimeter-Wave Communications,” *IEEE Trans. Wireless Commun.*, vol. 17, no. 2, pp. 752–765, 2018.